Chapter 1

DEM analysis of breakage behavior of bicomponent agglomerates

Maksym Dosta, Matthias Weber, Volker Schmidt, and Sergiy Antonyuk

Abstract The discrete element method (DEM) is an effective approach for the numerical investigation of micromechanical behavior of granules and agglomerates. In this chapter, we apply an extension of the DEM, the so-called bonded particle model (BPM), for modeling the breakage behavior of cylindrical and spherical multicomponent agglomerates during quasi-static compression. The considered agglomerates consist of ideally spherical primary particles connected by cylindrical solid bonds.

In several previous case studies, we investigated the behavior of agglomerates consisting of two different types of particles and solid bonds, where the simulations were performed on virtual microstructures generated by a stochastic agglomerate model. For this, we varied the volumetric ratio of both types of particles as well as their material properties. The results obtained show complex non-linear dependencies of the mechanical characteristics of agglomerates on their microstructure and composition.

Introduction

In this chapter, we investigate the breakage behavior of bicomponent agglomerates under uni-axial compressive load. Knowledge about breakage mechanisms is important for different fields of application. For example, production processes such as granulation and grinding depend on breakage characteristics of the used agglomerates. In recent years, increasing computational resources permit the investigation of mechanical properties based on simulation experiments. Various research has already been conducted to examine the relationship of agglomerate properties and their breakage behavior. For instance, in the case of impact breakage, the effect of agglomerate's shape and impact angle on breakage behavior has been investigated [Liu10].

The aim of this chapter is to quantify the relationship between the microstructure of agglomerates and their macroscopic breakage behavior. We consider agglomerates made up of a relatively dense packing of spherical primary particles connected by cylindrical bonds. We study the effect of different material properties of primary particles and bonds on breakage characteristics of these agglomerates. On the one hand, we consider agglomerates made up from equally-sized spheres and compare them to agglomerates made from two types of particles with different diameters. On the other hand, we take cylindrical agglomerates composed of a single type of spherical primary particles and vary the Young's modulus of the bonds. Again, we compare breakage characteristics

M. Dosta
Institute of Solids Process Engineering and Particle Technology, Hamburg University of Technology, Hamburg, Germany; e-mail: dosta@tuhh.de

M. Weber ● V. Schmidt
Institute of Stochastics, Ulm University, Germany;
e-mail: volker.schmidt@uni-ulm.de

S. Antonyuk
Institute of Particle Process Engineering, Technische Universität Kaiserslautern, Kaiserslautern, Germany;
e-mail: sergiy.antonyuk@mv.uni-kl.de

of agglomerates made up from bonds with the same Young's modulus to those of agglomerates made up from two types of bonds with different Young's moduli.

For the simulation, we apply the MUSEN framework [Dos13] which uses the discrete element method (DEM) and the bonded particle model (BPM) to simulate the time-resolved behavior of an agglomerate under compressive load. A general description of DEM and a detailed summary of literature dealing with the application of BPM for microscale modeling of agglomerates can be found in Chapter 4. The considered agglomerates are created using a stochastic model [Spe15] which is able to generate densely packed agglomerates of spherical primary particles with varying sizes. Furthermore, it incorporates the placement of cylindrical bonds between primary particles.

The simulation experiments considered in this chapter show a clear dependency of breakage properties such as breakage force and deformation on the composition of bicomponent spherical agglomerates. Homogeneous mixtures of both types of primary particles tend to exhibit a lower breakage force, but a higher deformation, indicating higher elasticity. For cylindrical agglomerates, we show that the Young's modulus of bonds plays an important role in the breakage behavior.

1. Methods

1.1 Agglomerate structure generation algorithm

The agglomerates under study consist of spherical primary particles and cylindrical solid bounds. This resembles typical structures obtained by industrial wet agglomeration processes such as pelletizing discs and tablet presses. For usage in DEM simulations, agglomerate structures are created in two stages [Spe15]. In the first stage, a packing of primary particles is generated; in the second stage, a set of solid bonds connecting the primary particles is added. To generate a packing of primary particles, the force-biased algorithm [Mos89] has been applied. In the first step of this algorithm, primary particles are randomly placed into a specified volume. In further iterations contacts between particles are detected and virtual forces in normal directions are calculated. Afterwards, the particles are moved according to the forces acting on them. Thereby, the inner stresses are reduced. Using this procedure, the overlaps between primary particles are reduced. The stiffness which is used to calculate the inter-particle forces is not directly related to material properties. It is calculated automatically in the algorithm and varies depending on the maximal particle velocity in the system. In order to avoid size or material dependent segregation of particles, their masses during generation are scaled. Additional conditions ensure that all particles are totally contained in the specified volume. For this purpose, a virtual wall representing the generation domain is considered. Interactions between particles and wall are taken into account when calculating the virtual forces acting on the particles. The rearrangement algorithm is stopped when the maximal overlap between particles and between particles and walls is smaller than some threshold value. In Fig. 1.a, an initial particle placement and the corresponding final packing are shown schematically.

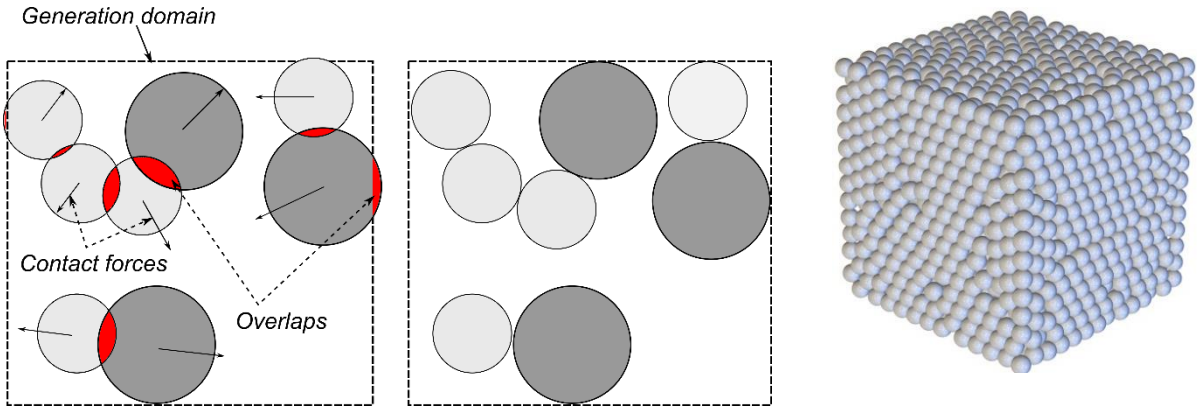

a) Arrangement of spheres before and after collective rearrangement by force-biased algorithm.

b) Pattern formation for high packing densities

Fig. 1. Generation of particle packing using the force-biased algorithm.

The proposed generation approach allows us to model homogeneous and isotropic structures for packings with high packing densities. This means that there is no preferred direction for e.g. contacts between particles and there is no spatial gradient in the packing density. These are reasonable assumptions for spherical agglomerates produced by e.g. spray granulation and we restricted ourselves to this case. However, non-homogeneous agglomerates occur in reality, too, e.g., agglomerates with spatially varying packing density or agglomerates having a core-shell structure. These could be modeled by extending the present approach, see Weber et al. (2017). Application of the developed algorithm for low packing densities will lead to the formation of spatially distributed particle clusters. In the case of very high packing densities the algorithm will result in ordered structures (see Fig. 1.b) and can lead to formation of fcc, bcc or hcp-like structures.

In the second stage, bonds are generated between primary particles. For this purpose, two different algorithms are used for the creation of cylindrical and spherical agglomerates. For the creation of cylindrical agglomerates, a simple algorithm based on a distance threshold is used. A bond between two primary particles is generated if the distance between those is smaller than a specific threshold. For case studies with spherical agglomerates, an advanced approach based on the volume fraction of binder material is applied. The aim is to connect the primary particles by bonds such that the union of all bonds has a given total volume. This volume is obtained as a volume fraction with respect to the total volume of primary particles. The idea is to construct an agglomerate where all particles being sufficiently close to each other are connected and further bonds are only inserted where necessary to obtain connectivity. Then, the volume of bonds can be controlled by the thresholding value used to connect particles. If this threshold is zero, only bonds necessary to obtain connectivity are generated. For larger thresholds, the number of bonds (and their total volume) is increased.

This can be implemented as an algorithm using ideas from graph theory [Jun08]. For a given distance threshold $l \geq 0$, we will construct a graph $G^{(l)} = \left(V, E^{(l)}\right)$ that connects the set of vertices (particles) V by the set of edges (bonds) $E^{(l)}$. A bond between two particles is only put if the smallest distance between their surfaces is less than or equal to l or if the bond is required for

complete connectivity, i.e., every primary particle has be connected directly or indirectly to all others via the bond system. Such a graph $G^{(l)}$ can be obtained by the following algorithm, which is illustrated in Fig. 2.

1. Compute the relative-neighborhood graph (RNG) [Tou80] $G^{(l)}_{RNG}$ of the primary particles, using a suitable distance function $d: V \times V \to [0, \infty)$ (see below). In the RNG, an edge is put between two vertices when there is no third vertex closer to both vertices (with respect to d). Using this technique, the vertices (primary particles) are always completely connected by the edges in the RNG [Tou80]. A suitable distance function d is given by

$$d\big((x,r),(x',r')\big) = \max\{0, ||x - x'|| - r - r' - l\}, \tag{1}$$

   where x and x' are the centroids of the considered particles and r and r' are their respective radii. As d is zero if the distance of the surfaces of two particles is at most l, the RNG contains all edges that connect two particles within a given distance l and further edges ensuring complete connectivity. Therefore, $G^{(l)}_{RNG}$ fulfills most properties desired for $G^{(l)}$, but it may contain more edges than necessary for connectivity. More precisely, it is a superset of the graph we are interested in, whose construction is explained in the next step.
2. Compute the minimum spanning tree (MST) [Jun08] $G^{(l)}_{MST}$ of $G^{(l)}_{RNG}$, again using the same distance function d given in (1), now applied to the existing edges. In the MST, as many edges as possible are deleted while minimizing the sum of distances and preserving connectivity.
3. The result $G^{(l)}$ is given by the edges of the graph $G^{(l)}_{MST}$ combined with all edges in $G^{(l)}_{RNG}$ having ”length” zero, i.e., the surfaces of the corresponding primary particles have at most a distance of l from each other.

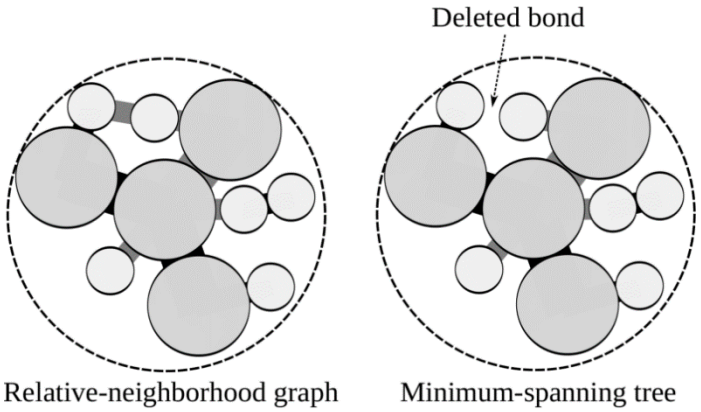

Fig. 2. Illustration of RNG for l = 0 and MST for the same graph [Spe15]. Direct contacts are shown in solid black, further connectivity bonds are gray.

Recall that for a given threshold value $l \geq 0$, $G^{(l)}$ is the graph connecting all particles that are within distance l to each other, plus further bonds that are required for connectivity. For a given set of primary particles, the binder volume fraction (which is given as a model parameter) can be converted into the absolute binder volume. The aim is to find the ‘optimal’ threshold value l^* such

that the absolute binder volume obtained from the connectivity graph $G^{(l)}$ is closest to the target value. This leads to a minimization problem

$$l^* = \arg\min_{l \geq 0} \left| \sum_{e \in E^{(l)}} volB(e) - b_{abs} \right|, \tag{2}$$

where b_{abs} is the absolute binder volume targeted and $volB(e)$ denotes the volume of the bond specified by edge e.

1.2 Contact models

For modeling of quasi-static compression of agglomerates, a bonded particle model (BPM) has been used [Dos16, Pot04]. Here three rheological contact models have been employed. The soft-sphere visco-elastic Hertz-Tsuju [Tsu92] model for normal force and the Mindlin model for tangential force [Min53] were used to describe particle-particle and particle-wall interactions [Dos18]. For modeling of the solid bonds, a rheological model of the ideally elastic material was applied. The forces and moments caused by bonds have been added to the interparticle interactions. One of the main limitations when applying BPM is a lack of detection and calculation of physical contacts between primary particles and solids bonds. This leads to the reduction of accuracy when the distance between surfaces of bonded particles is relatively large.

The relative motion of connected particles leads to a deformation of bonds and causes corresponding forces and moments. The force in the normal direction F_n is calculated directly from the current positions of primary particles. The force depends on the bond deformation ΔL and is calculated as

$$F_n(t) = \frac{\Delta L(t)}{L_{init}} \cdot A_b \cdot E\,, \tag{3}$$

where A_b is the bond cross-cut surface, L_{init} the initial bond length, and E the Young's modulus. The distance between particle centers is taken as bond length. For the calculations of force in tangential direction F_t as well as for torsional and bending moments M_n and M_t, respectively, an iterative approach is used. In each DEM simulation time step, the increment of force is calculated and added to the transformed previous value. For example, the tangential force in the global coordinate system for the new time step is computed as

$$F_t(t + \Delta t) = T \cdot F_t(t) + \frac{\Delta t \cdot v_{rel,t}}{L_{init}} \cdot A_b \cdot \frac{E}{2(1+\nu)}, \tag{4}$$

where ν is the Poisson ratio, $v_{rel,t}$ the relative velocity in tangential direction and T the rotation matrix to consider motion of contact partners in three-dimensional space.

In order to simulate agglomerate breakage the stresses acting in each individual bond are analyzed and compared with material properties for tension strength σ_{max} and shear strength τ_{max}. If one of the conditions given in Eq. 5 and 6 is fulfilled, the bond breaks and is removed from the simulation domain. Moreover, it is assumed that there is no compressive breakage of single

bonds. Therefore, the condition in Eq. 5 is only taken into account when the bond is elongated. Then, a bond breaks if either of the following conditions holds

$$\frac{F_n(t)}{A_b} + M_t \cdot \frac{R_b}{I} > \sigma_{max} \text{ or} \tag{5}$$

$$\frac{F_t(t)}{A_b} + M_n \cdot \frac{R_b}{J} > \sigma_{max}\,, \tag{6}$$

where R_b is the bond radius, I and J the area and polar moments of inertia, respectively.

For DEM calculations, the MUSEN simulation framework has been used [Dos13]. The calculations in this system are parallelized for computation on a graphic processor unit (GPU) using the CUDA library. This reduces computation time significantly, thus allowing to perform a large number of simulation studies. For parallelization of computations, atomic functions like *atomicAdd()* are used. Due to the formation of the internal queue of operands and the limited number of digits in floating point operands, the application of such functions leads to non-determenistic results. This means that two runs of the program on the same initial data will lead to varying results. However, the overall variations caused due to the usage of atomic operations are negligible in the investigated case studies.

2. Spherical agglomerate

2.1 Material parameters and agglomerate geometry

To begin with, we briefly recall the stochastic microstructure model introduced in [Spe15]. We denote the radius of a spherical agglomerate by r. The primary particles are also spheres and their radii are drawn from (independent copies of) a random particle radius R_p which takes values r_1 and r_2 with probabilities p and $1-p$, respectively. Thus, the agglomerate consists of particles of two different sizes. The volume fraction a (mixing ratio) of particles of radius r_1 is given by

$$a = \frac{p \cdot r_1^3}{p \cdot r_1^3 + (1-p) \cdot r_2^3}\,. \tag{7}$$

The targeted volume fraction of primary particles simulated inside the agglomerate is given by the packing density $\eta \in (0; \eta_{max}]$, where the maximal possible packing density η_{max} depends on the radius distribution of the primary particles (e. g., η_{max} = 0.74 for identical spheres).
The total volume of bonds is given as a ratio b > 0 with respect to the total volume of the primary particles. The bonds are cylindrical objects connecting two primary particles. The bond radius depends on the radius of the smaller adjacent particle: For a bond connecting two particles with radii r and r', the bond radius $\mathrm{r_b}$ is given by $\mathrm{r_b} = k_b \cdot \min\{r, r'\}$ for some factor $k_b \in (0; 1]$.
All parameters except the mixing ratio were fixed. The mixing ratio a was randomly chosen from the interval [0; 1]. The agglomerate radius was equal to 4 mm, radii of primary particles r_1 and r_2 were equal to 0.5 mm and 0.25 mm accordingly. The binder volume fraction was equal to 0.1 and bond radius factor k_b equal to 0.4.
Before investigating the breakage behavior of the agglomerates generated by the proposed stochastic model, it is interesting to look at some characteristics of the simulated microstructures. The agglomerate diameter as well as the porosity are always the same, but it is useful to analyze

the primary particle radii, coordination numbers and bond radii in dependence of the mixing ratio. For an optical impression, three agglomerates with different mixing ratios are shown in Fig. 3. The larger primary particles are visualized in blue, the smaller primary particles in yellow. For all three agglomerates one eighth has been cut out for visualization of the interior microstructure. For all evaluations, 300 agglomerates have been generated according to the stochastic microstructure model.

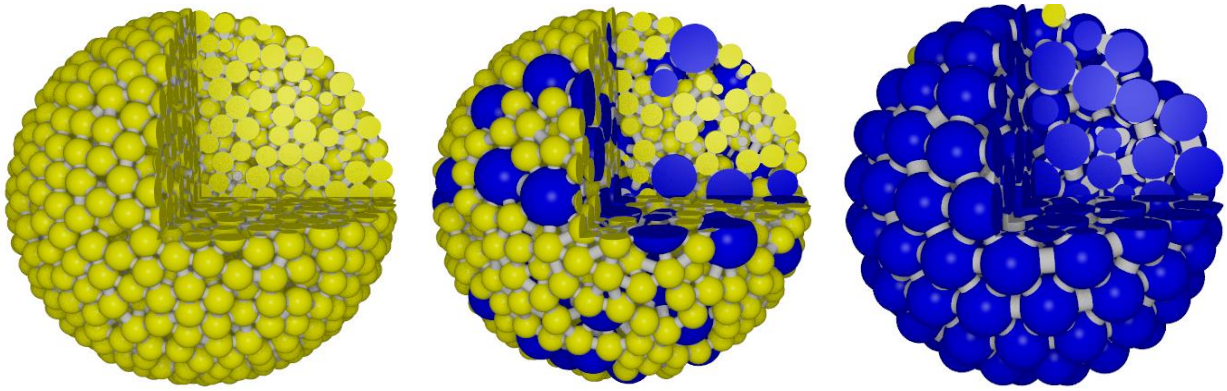

Fig 3. Three realizations of agglomerates for mixing ratios $a = 0$ (left), $a = 0.45$ (middle), and $a = 0.99$ (right) [Spe15].

The mean radius of primary particles (unweighted, i.e., not weighted by their volume or mass) clearly depends on the mixing ratio a. The average radius of particles in the agglomerate is calculated as

$$\bar{r} = \frac{N_1 r_1 + N_2 r_2}{N_1 + N_2}, \tag{8}$$

where N_1 and N_2 is the number of large and small particles respectively.
From the definition of volume fraction and considering the fact that $r_1 = 2r_2$ it can be derived that

$$a = \frac{N_1 r_1^3}{N_1 r_1^3 + N_2 r_2^3} = \frac{8N_1}{8N_1 + N_2}. \tag{9}$$

After substitution of Eq. 9 into Eq. 8, it follows that

$$\bar{r} = \frac{8 - 6a}{8 - 7a} r_2 . \tag{10}$$

In Fig. 4, the dependency of average diameter on volume fraction of larger particles is shown. The data obtained from the stochastically generated structure is visualized with circles and the theoretical approximation with a solid line. It can be observed that, due to the relatively large number of primary particles in agglomerate, the mean radius in probability-based generated structure is in good agreement with theoretical calculations.

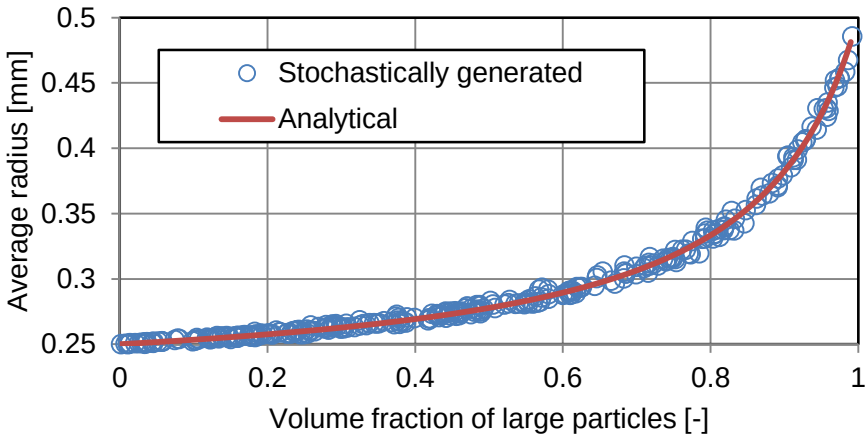

Fig. 4. Effect of mixing ratio on the average radius of primary particles in agglomerate.

However, the behavior of the coordination numbers, i.e., the number of bonds per primary particle, is more interesting. A larger value of the mean coordination number implies that the system of particles is better connected.

Fig. 5 shows that the mean coordination number is a bit smaller for very small and very large mixing ratios a than for intermediate `mixing' scenarios. On the other hand, the standard deviation (SD) is obviously largest in the range of $a \in [0.6; 0.8]$, where it achieves a value of almost 4 in comparison to about 2 for very low/high mixing ratios. This can be interpreted as a higher variability of the microstructure.

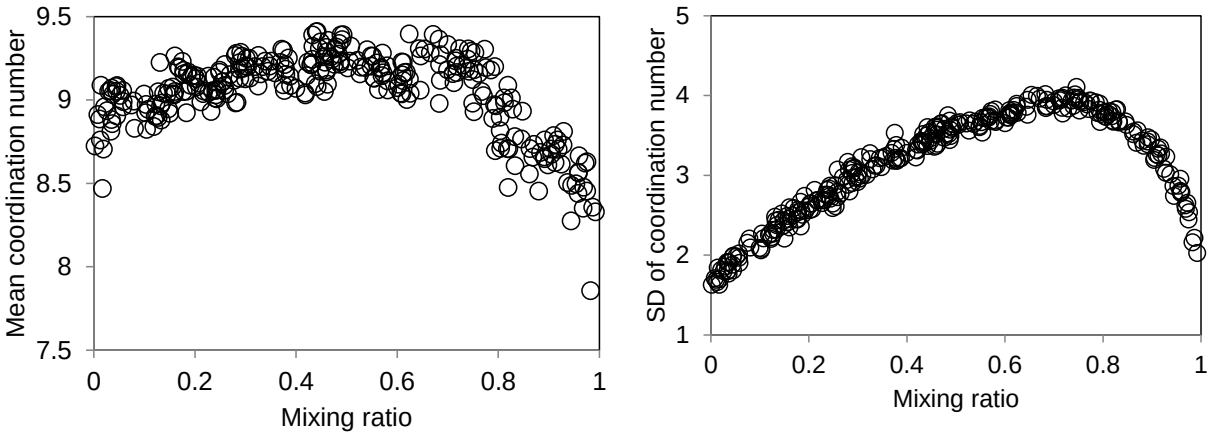

Fig. 5. Effect of mixing ratio on the coordination numbers of primary particles: mean coordination number (left), standard deviation of coordination numbers (right) [Spe15].

In combination with DEM simulations, the presented microstructure model can be used to investigate the relationship of structural and mechanical properties of agglomerates. The first step in order to achieve this goal is the description of real agglomerates using the given model, which has been done in [Spe16]. In this way, we obtain model parameters representing real agglomerates. Further research leads to the exploration and statistical analysis of breakage properties [Spe17]. However, one limitation of the presented model is the restriction to homogeneous and isotropic structures. While there are many types of particles for which these are reasonable assumptions, our model can easily be extended to overcome these shortcomings.

An extension to agglomerates which can be spatially separated into core and shell can be found in [Web17].
Agglomerate strength can be described partly by two important characteristics, see Fig. 6 (top). The maximum force applied before breakage is smaller for mixing scenarios (scenarios where both fractions of particle sizes are relevant) than in the uniform cases. A possible reason is the higher variability in agglomerates with both small and large particles. This leads to more weak points in the microstructure, where forces are not evenly spread and individual bonds are heavily loaded. Therefore, local fracturing occurs before a high (global) force is applied. This implicates that even for almost only small primary particles the force is considerably higher.
On the other hand, the (mass-related) primary breakage energy does not show this behavior. It seems to increase almost linearly with the mixing ratio, i.e., agglomerates consisting of larger primary particles and thicker bonds are more stable. This means that even though the maximum force is smaller for mixing scenarios, this does not influence the energy required for breakage. Therefore, the average force before breakage has to be similar or the related deformation has to be larger. Fig. 6 (bottom) shows the deformation of the agglomerates relative to their original diameter. It can be seen that the deformation at the breakage point really tends to be larger for mixing scenarios, but the fluctuations are in a wide range for all mixing ratios.

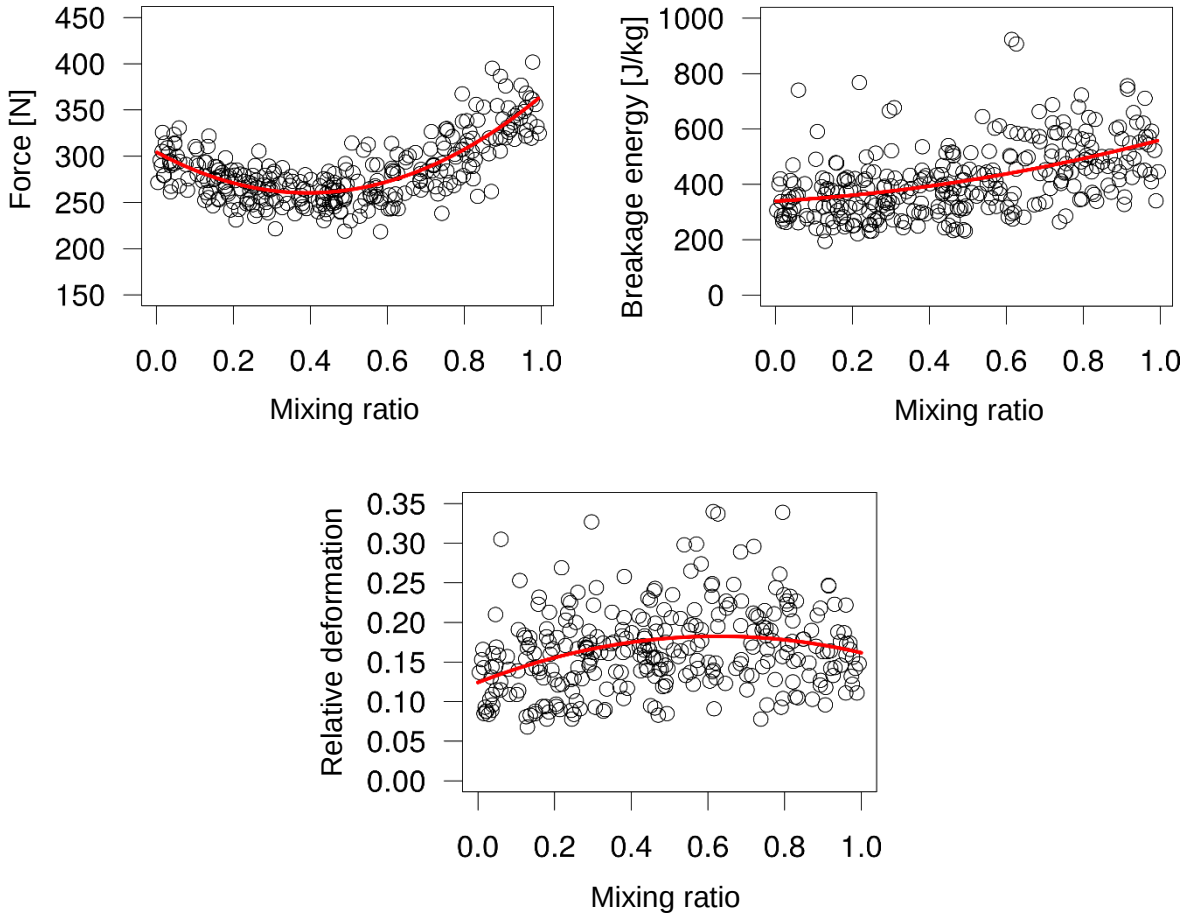

Fig. 6. Effect of mixing ratio on breakage behavior, i.e., on breakage force (top left), breakage energy (top right) and relative deformation (bottom) [Spe15].

3. Cylindrical agglomerate

3.1 Agglomerate geometry and material properties

The radius and height of the investigated cylindrical agglomerates are equal to 10 mm and 20 mm, respectively. Each agglomerate consists of 7200 primary particles with radius 0.5 mm connected by almost 29000 solid bonds with radius 0.25 mm. In Fig. 7, an agglomerate and its internal structure are shown. The previously described force-biased packing algorithm (see Section 1.1) has been used to create the agglomerates. In order to minimize the error which is caused due to the stochastic particle placement, ten different agglomerates have been generated and analyzed.

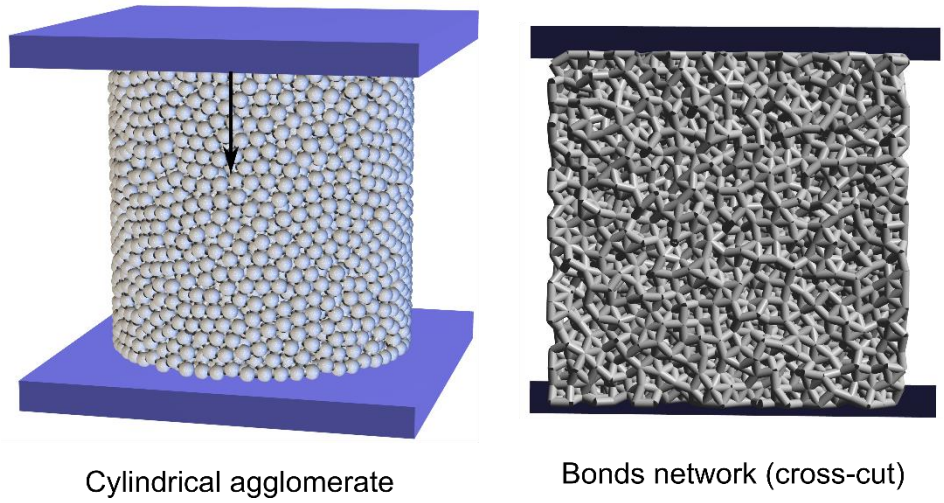

Fig. 7. Cylindrical agglomerate under uniaxial compression test.

The initial packing density of primary particles was equal to 0.63 which is almost equal to the density of a random close packing. The friction coefficient between primary particles and particles as well as between walls was set to 0.3. To analyze the influence of the distribution of particles and solid bonds on mechanical behavior, four model materials have been defined: two materials M_A and M_B for primary particles and two materials M_C and M_D for solid bonds. Most relevant material parameters are listed in Table 1. The parameters of materials M_A and M_C were kept constant whereas the parameters of materials M_B and M_D have been varied. For these, the range of variation is given in Table 1.

Table 1. Basic material parameters of materials M_A and M_B for particles, M_C and M_D for bonds.

	Particles		**Bonds**	
	M_A	M_B	M_C	M_D
Young's modulus [GPa]	2.5	[0.25-2]	0.02	[0.002-0.08]
Poisson ratio	0.2	0.2	0.2	0.2
Normal and shear strength [MPa]	-	-	0.5	0.5
Density [kg/m^3]	2500	2500	-	-

First, we studied the influence of the Young's modulus of bond materials on the deformation and breakage behavior for agglomerates containing only one type of binder M_D and one type of

particles M_A. In Fig. 8, typical force-displacement characteristics obtained for two different Young's moduli of solid bonds ($E = 40\ MPa$ and $E = 10\ MPa$) are illustrated. One can observe a linear elastic deformation behavior of the agglomerate almost until the breakage point. However, the force does not decrease suddenly after the primary breakage, indicating a viscous failure. From the obtained results it can be observed that the increase of the Young's modulus of the bonds decreases the agglomerate stiffness by factor four and the breakage displacement by about factor three. This non-linear dependency between the stiffness of binder material and final stiffness of agglomerate is caused by the agglomerate's internal structure. A more detailed analysis is given in Section 3.3 below.

The difference in failure strain is caused by the fact that the strength values of the bonds were kept constant. Thus for the case of the higher Young's modulus of bonds $E = 40\ MPa$, the same axial strain of the agglomerate leads to larger stresses in the bonds and as a consequence to earlier breakage. Because of the materials' strength being equal, the breakage force in both cases had an almost identical value of about 215 N.

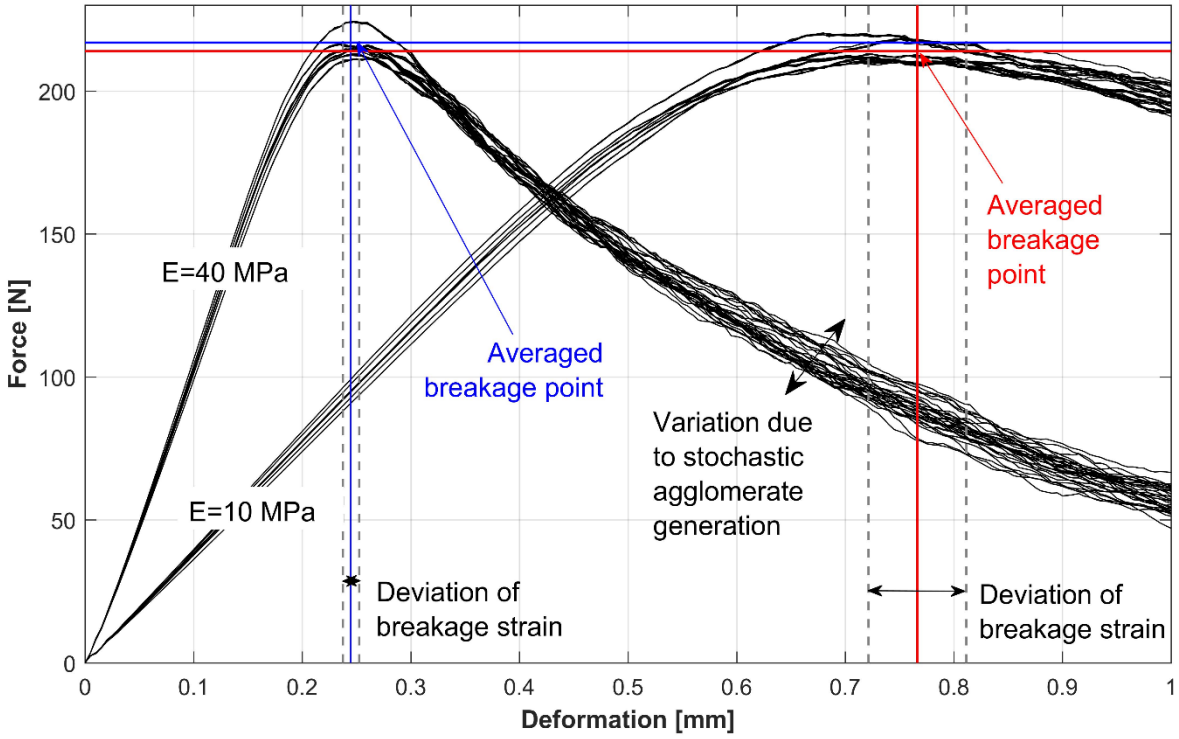

Fig. 8. Force displacement characteristics for agglomerates with varying bond stiffness.

The obtained results show that variations due to the stochastic generation of the microstructure of agglomerates are relatively small. The large number of primary particles, their high connectivity and high packing density result in a similar microstructure for all agglomerates.

3.2. Multicomponent bonds

In order to investigate agglomerates with multicomponent binder, heterogeneous bond networks consisting of two bond materials M_C and M_D have been generated. The fraction of bonds of material M_D in the total agglomerate is given by

$$K_{DC,N} = \frac{N_D}{(N_C + N_D)}, \tag{11}$$

where N_D and N_C are the total numbers of bonds of component M_C and M_D respectively.

Recall that in this case study it is supposed that all material parameters of bonds except for the Young's moduli are equal. The ratio of Young's moduli of materials M_D (E_D) and M_C (E_C) is described

$$K_{DC,E} = \frac{E_D}{E_C}. \tag{12}$$

According to the parameter $K_{DC,N}$, bonds of materials M_D and M_C have been created between primary particles. Both components have been distributed at random within all 10 initial agglomerates. For reduction of the statistical error caused by the random spatial positioning of bonds, five random agglomerates have been created for each initial agglomerate and value of $K_{DC,N}$. Therefore, the total number of investigated agglomerates for each specified set of parameters $K_{DC,E}$ was equal to 50.

The internal structure of agglomerates with different numbers of bonds of different types is illustrated in Fig. 9. Here, the cross sections of cylindrical agglomerates are shown and all particles are hidden.

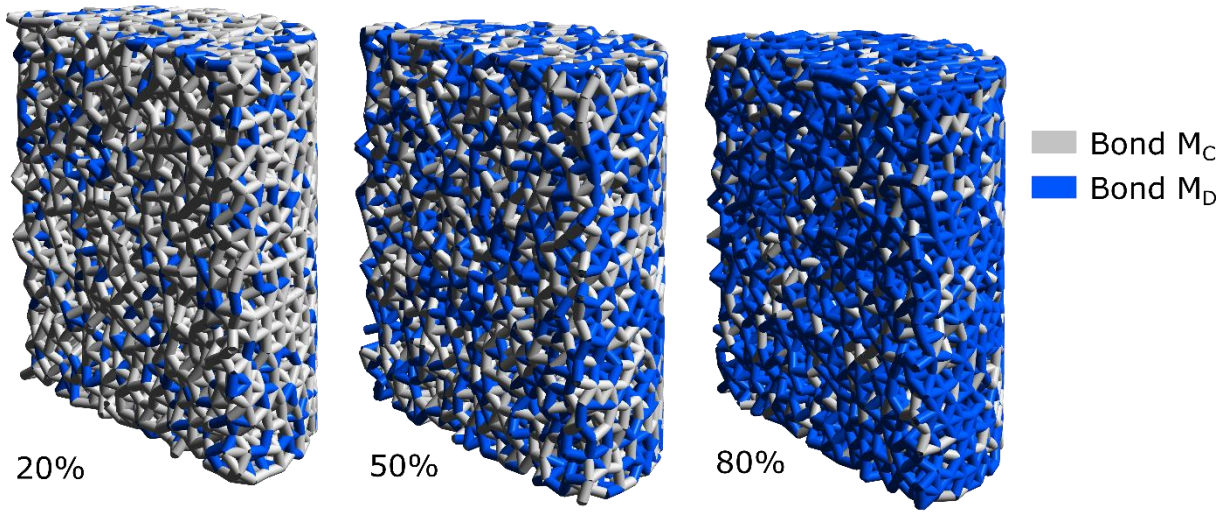

Fig. 9. Cross sections of internal structures of agglomerates with varied mixture of bond components. For better perceptibility of the bond network, primary particles are hidden.

In Fig. 10, the main mechanical characteristics obtained from the simulations of cylindrical agglomerates with varied content of bonds of type M_D (i.e., with different ratios $K_{DC,N}$) and varied Young's moduli (i.e., with different ratios $K_{DC,E}$) are shown. The values are averaged over force-displacement data of about 1500 simulated compression tests.

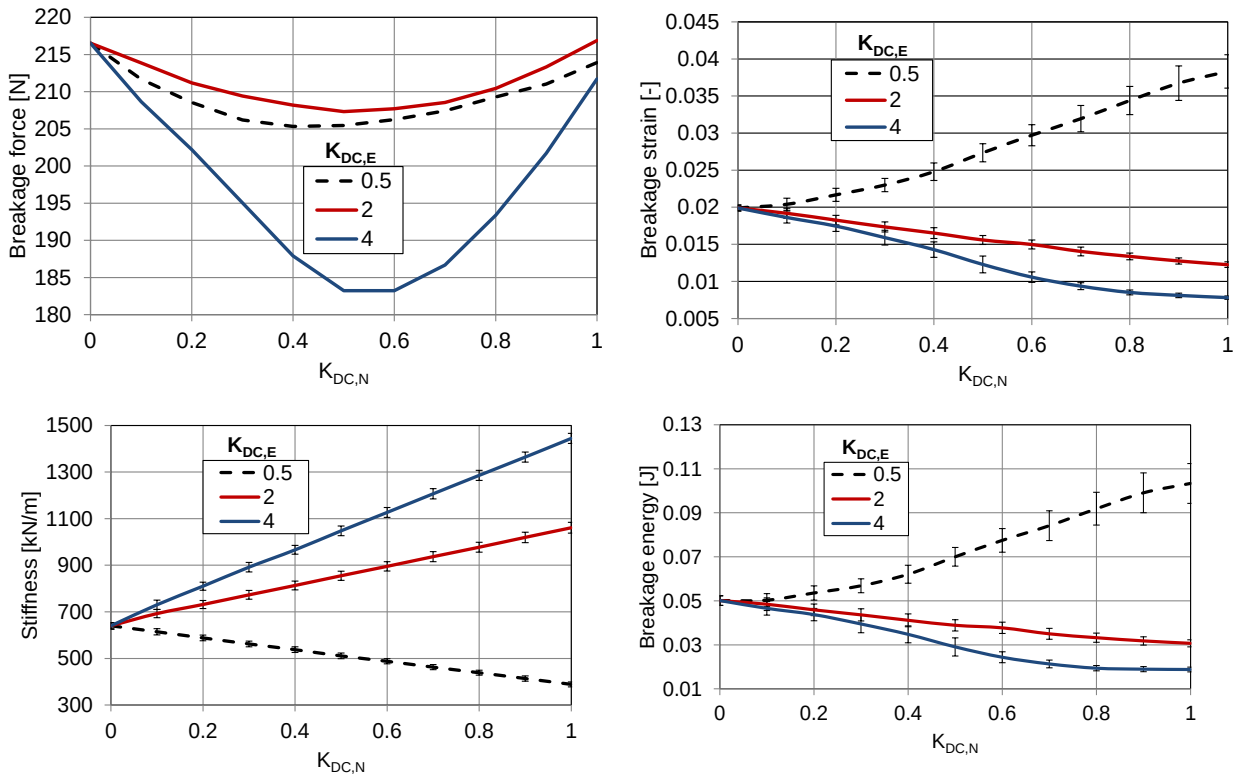

Fig. 10. Mechanical properties of multicomponent agglomerates with varied binder content and Young's modulus.

The upper left graph in Fig. 10 shows the dependency of breakage force on bond composition and Young's modulus. By the fact that the breakage strength of materials M_C and M_D was equal, it can be seen that the breakage force is almost independent on the stiffness of bonds. In the cases when all bonds consist of material M_C ($K_{DC,N} = 0$) with Young's modulus equal to 20 MPa or when all bonds consisting of material M_D ($K_{DC,N} = 1$) with Young's moduli 10 MPa, 40 MPa or 80 MPa, the breakage force is almost equal to about 215 N. A significant decrease of the breakage force is observed when both types of bonds are mixed together. This happens due to the non-homogeneous stress distribution in the agglomerates. The largest part of total mechanical stress in the agglomerates is distributed over the bonds with higher stiffness, which are subject to higher loads in comparison to bonds in agglomerates consisting of only one material. Agglomerates with the largest ratio of Young's moduli $K_{DC,E} = 4$ consisting of the same amount of bonds of both types M_C and M_D ($K_{DC,N} \approx 0.5$) exhibit the minimal breakage force of about 183 N.

The stiffness of agglomerates with multicomponent bonds depends almost linearly on the amount of bonds $K_{DC,N}$ (lower left graph of Fig. 10). A larger amount of bonds with higher stiffness results in increased overall stiffness of the total agglomerate. As a consequence, the breakage strain as well as the breakage energy decreases (right column of Fig. 10).

3.3 Stiffness ratio of bond to particle

In this section, the mechanical properties of cylindrical agglomerates consisting of particles of type M_A and bonds of material M_D are investigated. We analyzed the influence of the ratio between Young's moduli of bonds (E_D) and particles (E_A) on the mechanical properties. This ratio is denoted

as $K_{DA,E} = E_D/E_A$. For the simulations, the Young's modulus of particles was kept constant at 25 GPa and the modulus of bonds was varied between 0.2 and 80 MPa. The average coordination number (i.e., the number of bonds per particle) was equal to 4.02. In Fig. 11, the main mechanical characteristics obtained from simulation of quasi-static uni-axial compression of cylindrical agglomerates are shown. On the left-hand side, the influence of the Young's modulus of bonds on agglomerate stiffness and breakage strain is shown. On the right-hand side, the typical force-displacement characteristics for two specific values of $K_{DA,E}$ are illustrated.

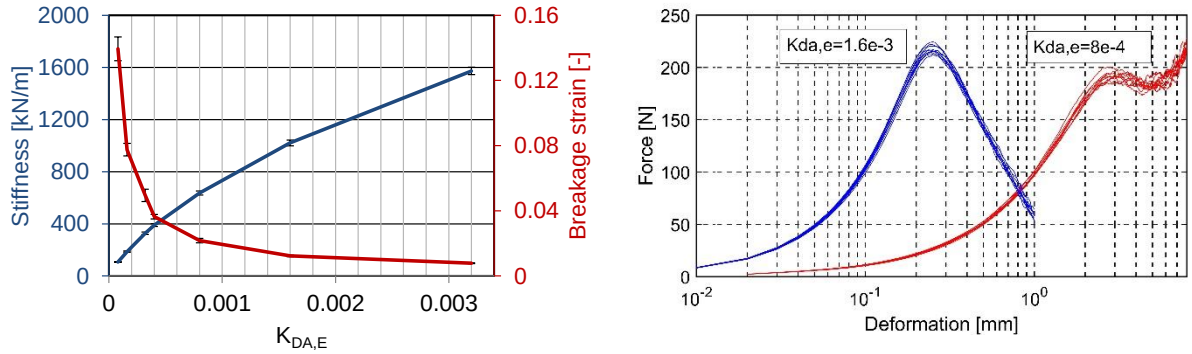

a) Averaged mechanical characteristics b) Typical force-displacement curves

Fig. 11. Simulation results for case studies with varied Young's modulus of bonds.

The increase of the Young's modulus of bonds leads to a non-linear increase of the stiffness of the whole agglomerate. When the bonds become stiffer, fewer contacts between primary particles are formed under compression, resulting in a reduced effect of particle contacts on the total agglomerate stiffness. In the investigated parameter domain, the stiffness of the agglomerate K_{agg} can be effectively described using the potential function

$$K_{agg} = 15.721[m] \cdot E_D^{0.729}\,, \tag{13}$$

Moreover, from Fig. 11 it can be observed that an increase of the Young's modulus of solid bonds E_D leads to a significant decrease of the breakage strain ε. Using the potential function, this dependency can be approximated by

$$\varepsilon = 2078.5\left[\frac{1}{Pa}\right] \cdot E_D^{0.789}\,. \tag{14}$$

Higher stiffness of solid bonds results in a more brittle breakage pattern. In Fig. 12 (left) force displacement characteristics for two typical agglomerates with parameters $K_{DA,E} = 1.6 \cdot 10^{-4}$ and $K_{DA,E} = 8 \cdot 10^{-4}$ are shown. The loading and unloading phases are shown using solid lines and dashed lines, respectively.

In the case of agglomerates with higher Young's modulus of bonds, a primary breakage point at a deformation of about 450 µm can be observed. Further increase of the load on the sample leads to the destruction of a large amount of solid bonds and consequently to a rapid decrease of the force. Only a small elastic recovery during unloading phase of the broken agglomerate (Fig. 12, left) can be observed. On the right-hand side of Fig. 12, an agglomerate structure colored according to the size of fragments is shown. The deformation behavior during failure indicates shear dominated fracture pattern.

In contrast, the simulated force-displacement curve of the agglomerate with softer bonds did not show a clear primary breakage point with a rapid drop of the force after the point of maximum force. Only a relatively small amount of bonds is destroyed. The sample exhibits a large elastic unloading. Therefore, even after a large deformation of about 2 mm (strain of 0.1), the general structure of the agglomerate remains stable and the sample recovers to its initial height.

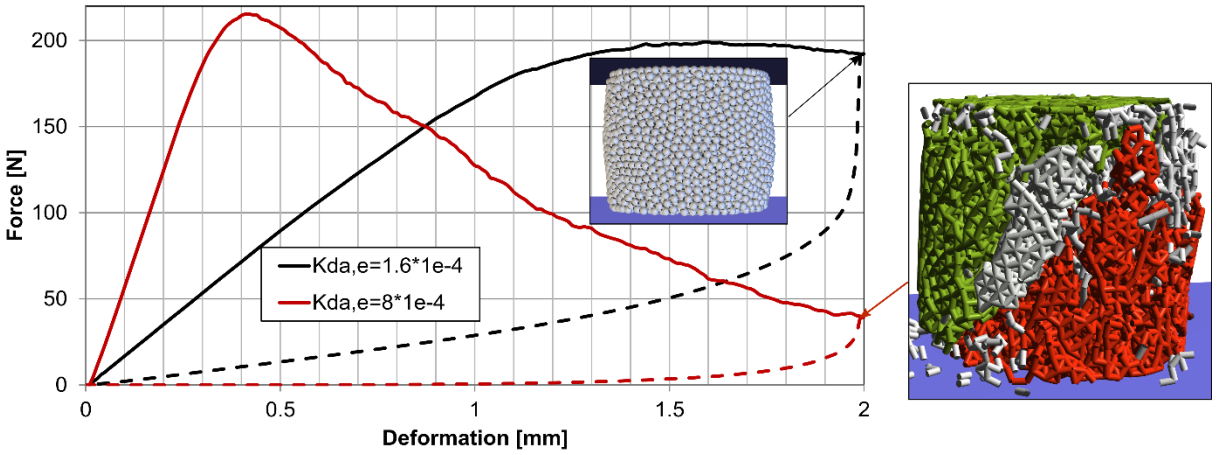

Fig. 12. Left: Influence of the bond stiffness on the force-displacement characteristics of agglomerates. Right: Bond network of sample agglomerate with Young's modulus 20 MPa after breakage. The largest and second largest fragments are shown in green and red, respectively; other fragments (debris) are shown in gray.

3.4 Bicomponent particle distribution

In this section, the mechanical characteristics of agglomerates which consist of two types of primary particles are analyzed. The primary particles have a constant diameter of 2 mm and differ only in their stiffness. The number fraction of particles of material M_B in the agglomerate is described by

$$K_{BA,N} = \frac{N_B}{(N_B + N_A)}, \tag{15}$$

where N_A and N_B are the total numbers of particles of materials M_A and M_B, respectively. Since the sizes of primary particles are equal, the parameter $K_{BA,N}$ also describes the volume fraction of particles of material M_B.

It was supposed that all material parameters of particles apart from Young's moduli were equal. The ratio of Young's moduli of material M_B (E_B) and M_A (E_A) was described by

$$K_{BA,E} = \frac{E_B}{E_A}, \tag{16}$$

In our simulations, the Young's modulus of material M_A was kept constant while material M_B was chosen softer than material M_A, resulting in $K_{BA,E} < 1$. The (number) fraction of particles of material

B was varied between 0 and 1 for five different values of $K_{BA,E}$. In Fig. 13, the approximated overall stiffness of the agglomerate is shown. As expected, the volume fraction and stiffness of the softer component directly influence the agglomerate stiffness. Higher volume fraction and decreased stiffness of the softer primary particles, both result in a reduced overall stiffness of the agglomerate. When the difference between Young's moduli of both components is relative small, the dependency between stiffness of the agglomerate and volume fraction of the second component can be roughly approximated by a linear function. However, a further decrease of E_B leads to non-linear dependency.

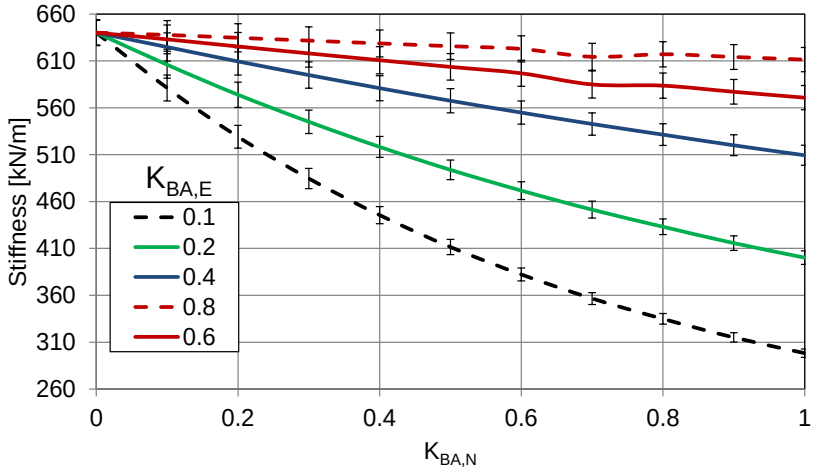

Fig. 13. Influence of the volume fraction $K_{BA,N}$ and stiffness $K_{BA,E}$ of softer primary particles on the agglomerate's total stiffness.

Conclusion

In this chapter, the discrete element method and the bonded-particle model have been applied to investigate the mechanical properties of cylindrical and spherical bicomponent agglomerates under quasi-static compression. Four cases have been analyzed:

- large and small particles of the same material (spherical agglomerates);
- solid bonds of two different materials (cylindrical agglomerates);
- varied stiffness ratio of bonds to particles (cylindrical agglomerates);
- primary particles of two different materials (cylindrical agglomerates).

The obtained results show that the microstructure and composition of bicomponent aggregates have a significant influence on their mechanical properties such as stiffness or strength. For example, the breakage force of cylindrical agglomerates with two different bond materials reveals a distinctive minimum for specific mixtures. This occurs due to the large heterogeneity of the stresses inside the bond network. Furthermore, a complex non-linear behavior can be also observed in the case when agglomerates consist of primary particles of different sizes. Here, the breakage force strongly depends on the mixing ratio and reaches its minimum for ratios of about 50%.

It should be mentioned that correlations and conclusions given in this chapter are valid only for a strictly limited parameter domain. It is expected that significant changes of material properties can result in a different material behavior.

Literature

[Dos13] M. Dosta, S. Antonyuk, S. Heinrich (2013). Multiscale simulation of agglomerates breakage in fluidized beds, *Ind. Eng. Chem. Res.* 52, 11275-11281.

[Dos16] M. Dosta, S. Dale, S. Antonyuk, C.R. Wassgren, S. Heinrich, J.D. Litster (2016). Numerical and experimental analysis of influence of granule microstructure on its compression breakage, Powder Techn. 299, 87-97.

[Dos18] M. Dosta, U. Bröckel, L. Gilson, S. Kozhar, G.K. Auernhammer, S. Heinrich (2018). Application of micro computed tomography for adjustment of model parameters for discrete element method, *Chem. Eng. Res. Design 135, 121-128.*

[Jun08] D. Jungnickel (2008). Graphs, Networks and Algorithms, 3rd Edition, Springer, Berlin.

[Liu10] L. Liu, K. Kafui, C. Thornton (2010). Impact breakage of sperical, cuboidal and cylindrical agglomerates, *Powder Techn.* 199 (2), 189-196.

[Min53] R.D. Mindlin, H. Deresiewicz (1953). Elastic spheres in contact under varying oblique force, *Trans. ASME, J. Appl. Mech* 20, 327-344.

[Mos89] J. Mościński, M. Bargieł, Z. A. Rycerz, P. W. M. Jacobs (1989). The force-biased algorithm for the irregular close packing of equal hard spheres, *Mol. Simulat. 3 (4), 201-212.*

[Pot04] D.O. Potyondy, P.A. Cundall (2004). A bonded-particle model for rock, *Int. J. Rock Mech. Min. Sci. 41, 1329-1364.*

[Spe15] A. Spettl, M. Dosta, S. Antonyuk, S. Heinrich, V. Schmidt (2015). Statistical investigation of agglomerate breakage based on combined stochastic microstructure modeling and DEM simulations, *Adv. Powder Tech. 26, 1021-1030.*

[Spe16] A. Spettl, S. Bachstein, M. Dosta, M.Goslinska, S. Heinrich, V. Schmidt (2016). Bonded-particle extraction and stochastic modeling of internal agglomerate structures, *Adv. Powder Tech. 27, 1761-1774.*

[Spe17] A. Spettl, F. Klingner, M. Dosta, S. Heinrich, V. Schmidt (2017). Copula-based approximation of particle breakage as link between DEM and PBM, *Comput. Chem. Eng. 99, 158-170.*

[Tsu92] Y. Tsuji, T. Tanaka, T. Ishida (1992). Lagrangian numerical simulation of plug flow of cohesionless particles in a horizontal pipe, *Powd. Techn.* 71, 239-250.

[Tou80] G. T. Toussaint (1980). The relative neighbourhood graph of a finite planar set, *Pattern Recogn. 12, 261-268.*

[Web17] M. Weber, A. Spettl, M. Dosta, S. Heinrich, V. Schmidt (2017) Simulation-based investigation of core-shell agglomerates: influence of spatial heterogeneity in particle sizes on breakage characteristics, *Comp. Mater. Sci. 137, 100-107.*